FISEVIER

Contents lists available at ScienceDirect

Current Opinion in Solid State & Materials Science

journal homepage: www.elsevier.com/locate/cossms





Pathways to controlled 3D deformation of graphene: Manipulating the motion of topological defects

Emil Annevelink^a, Harley T. Johnson^{a,b}, Elif Ertekin^{a,*}

- ^a Department of Mechanical Science and Engineering, University of Illinois at Urbana-Champaign, Urbana, IL 61801, USA
- ^b Department of Materials Science and Engineering, University of Illinois at Urbana-Champaign, Urbana, IL 61801, USA

ARTICLE INFO

Keywords:
2D materials
3D deformations
Topological defects
Migration pathways
Deep learning
Forward and inverse problems

ABSTRACT

Functional properties of 2D materials like graphene can be tailored by designing their 3D structure at the Angstrom to nanometer scale. While there are routes to tailoring 3D structure at larger scales, achieving controllable sub-micron 3D deformations has remained an elusive goal since the original discovery of graphene. In this contribution, we summarize the state-of-the-art in controllable 3D structures, and present our perspective on pathways to realizing atomic-scale control. We propose an approach based on strategic application of mechanical load to precisely relocate and position topological defects that give rise to curvature and corrugation to achieve a desired 3D structure. Realizing this approach requires establishing the detailed nature of defect migration and pathways in response to applied load. From a computational perspective, the key needed advances lie in the identification of defect migration mechanisms. These needed advances define new forward and inverse problems: when a fixed stress or strain field is applied, along which pathways will defects migrate?, and vice versa. We provide a formal statement of these forward and inverse problems, and review recent methods that may enable solving them. The forward problem is addressed by determining the potential energy surface of allowable topological configurations through Monte Carlo and Gaussian process models to determine defect migration paths through dynamic programming algorithms or Monte Carlo tree search. Two inverse models are suggested, one based on genetic algorithms and another on convolutional neural networks, to predict the applied loads that induce migration and position defects to achieve desired curvature and corrugation. The realization of controllable 3D structures enables a vast design space at multiple scales to enable new functionality in flexible electronics, soft robotics, biomimetics, optics, and other application areas.

1. Introduction

Two-dimensional materials offer new functionality due to their atomic-scale thickness and fully-coordinated atomic bonding. This combination leads to novel design methods in 2D materials like graphene. A unique feature of graphene is that it can undergo large out-of-plane deformations, enabling 3D corrugation and reconfiguration. Because of the large difference in rigidity for in–plane [1] and out–of–plane [2,3] deformation, the presence of internal strain induces 3D reconfigurations. For instance, topological defects known as disclinations are non-existent in bulk materials, but form in 2D materials due to their ability to deform out-of-plane. Such 3D features can be used to tune electronic, chemical, and mechanical properties, providing vast degrees of freedom in the design space. However, there are no mechanisms yet that achieve controlled out-of-plane deformation at the

Angstrom to nanometer scale.

Many novel properties reported in 2D materials result from their ability to deform out-of-plane. Controlled 3D deformation in 2D materials can tailor functional properties such as mechanical toughness, optical band gap, thermal transport, and pseudomagnetic fields [4–6]. Each of these arise from local strains that are present and induce a 3D structure that alters the engineering properties. For instance, the K_{1C} fracture strain of graphene is nearly tripled, due to crack deflection and bridging in 3D sinusoidal deformation as compared to flat [7]. Or, nanometer scale 3D deformation, which are on the length scale of the building blocks of life (proteins, carbohydrates, nucleic acids, and lipids), significantly impacts the properties of biological materials due to better adhesion and interaction [8–10].

One of the principal assumptions of each of these examples is that 3D deformation and curvature occurs at the atomic scale (1-10 nm). While

E-mail address: ertekin@illinois.edu (E. Ertekin).

^{*} Corresponding author.

recent work has shown that crinkle formation can create sharp features [11], ruga-mechanics based methods of the substrate typically result in features at larger length scales [12,13]. Utilizing substrates to selectively create ripples through uniaxial and biaxial compression [14–16] yields ripples having wavelengths of hundreds of nanometers limiting the amount of strain localization that occurs due to 3D deformation [17,18]. Additionally, further compression of the substrates lead to delamination causing crumpling and fold generation [19,20]. While selective delamination has created an entire new area of study for creating novel 3D sensors using 2D materials, the periodic feature size of devices still remains at the micron scale [21–23]. In order to create 3D deformations at the atomic scale, a different method that can create localized deformation is needed.

A promising approach is the controlled introduction of patterned in-plane (internal) strain. When built-in internal strains are introduced to 2D materials constrained to be flat, the in-plane accommodation of strain gives rise to large local stresses. When released, 2D materials can buckle out-of-plane, adopting 3D configurations that relieve stress to the extent possible. Out-of-plane deformation results in a regular 3D structure with controlled features and curvature at the desired scale (see Fig. 1(a)). Internal strains can be introduced in many ways. One approach is through in-plane heterostuctures of 2D materials. The strain caused by the lattice mismatch of two materials causes nanometer bending and curvature [24-26]. However, this approach to control is reliant on creating atomically sharp interfaces between materials during growth [27,28]. Shape programming of 2D transition metal dichalcogenides by patterned alloying could yield dynamic and reversible shape changes by including components that respond to stimuli [29]. Here, the synthesis of these materials requires a patterned substrate, which limits the resolution to feature sizes achievable with lithography. Atomic scale 3D deformation is also possible by altering the internal strain of 2D materials through precise patterning of topological defects and their position [30]. The goal is to create 3D structures like hemispheres, ridges, and hills using topological defects that each have a unique 3D deformations (see Fig. 1(b)). For internal strain engineering via topological defects, there exist formulations of the forward problem (viz. given a topological defect distribution, find the resulting 3D structure) [31] and the inverse problem (viz. given a desired 3D structure, identify the defect distribution) [7].

What is missing is a path to achieving the desired spatial distribution of topological defects. Deterministic control over topological defects – their positions and arrangement – in 2D materials would overcome a critical bottleneck to control of 3D deformation in 2D materials and allow access to new frontiers in device engineering applications. In this paper, we review the state of the art in accomplishing this goal and propose necessary advances to achieve it. We suggest that strategically applied loads – prescribed tractions and displacements of the 2D material – can be used to achieve the desired control. In Section 2, we first review an established framework that connects topological defects to 3D deformation. We then summarize earlier computational efforts to describe defect formation and evolution (Sections 3.1,2,3.2), and present a formal description of the challenges faced when seeking to control the spatial distribution of topological defects (Section 3.3). Finally, we

propose computational approaches that may help overcome these challenges (Section 4). The path to control of topological defects in 2D materials is based on determining (1) the mechanisms of topological defect formation and migration and (2) the applied load that will evolve a given distribution of topological defects to a target distribution. Our proposal is associated with its own *meta* forward and inverse problem: given that a mechanical load is applied to a 2D material, along what pathway will topological defects evolve and what resting position will they ultimately adopt, and vice versa. We close with by considering how this computational approach can be validated by and extended to experiments (Section 5).

2. 3D design from topological defects

The notion of topological defects arose from homotopy theory in the field of algebraic topology [32], and is closely related to the concept of geometric frustration in crystals [33]. A defect is a tear in the order parameter field (here the atomic displacements), and a topological defect is a tear that cannot be patched using only local rearrangements. For instance, no amount of reshuffling of atoms can 'fix' the fact that more rows of atoms enter from one side than leave the other side of a circuit encircling an edge dislocation [34]. Although algebraic topology is an old field, the application of topological defects to condensed matter systems itself originated in the 1970's (nematic liquid crystals [35], superfluid helium [36], and metallic glasses [37,38]). Topological defects are invoked in a theory of melting in 3D crystals [39,40] and flexible 2D membranes [41], in which melting occurs by a destruction of crystalline order as defects proliferate.

As illustrated in the work of Seung and Nelson [42], a key distinction between 2D and 3D is that the strain field surrounding a topological defect in 2D can be relieved by buckling out of plane: 2D membranes deforming in a 3D world can trade stretching energy for bending energy. This is quantified in the Föppl-von Kármán parameter γ : the ratio of inplane stiffness to out-of-plane bending stiffness, where materials with large γ (e.g. 2D materials) more easily bend and crumple than stretch and shear [43,44]. The large reduction in the distortion energy that occurs through buckling is responsible for the prevalence of these defects in 2D. For instance, the distortion energy of a disclination diverges linearly with system size in 3D, but the divergence is reduced to logarithmic in 2D. Similarly, the distortion energy of a dislocation (a bound disclination pair) diverges logarithmically with size in 3D, but becomes finite-valued in 2D [42]. Although we focus on the role of the large Föppl-von Kármán parameter of 2D materials for 3D deformation from topological defects, we note that it also makes them good candidates for kirigami based devices [45,46].

2.1. Disclinations and dislocations

Topological defects impart internal strain to the lattice by breaking the ground-state lattice symmetry of the pristine crystal. The principal defects are disclinations and dislocations. Each topological defect has a characteristic 3D deformation, the set of which forms a basis set for 3D deformations in 2D materials (see Fig. 1(d-f)). The 3D deformation of a

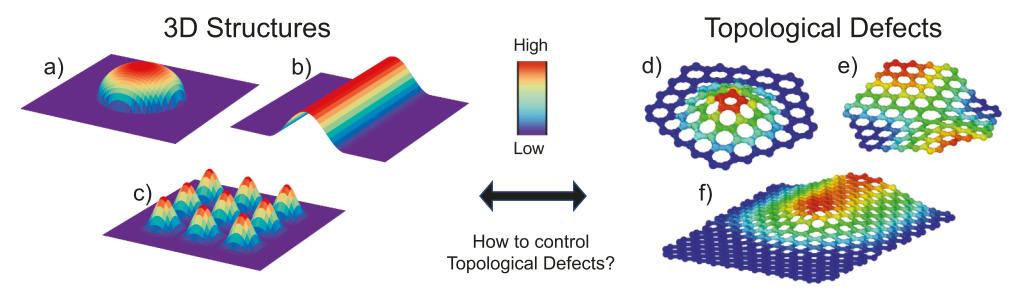


Fig. 1. The three-dimensional design of two-dimensional materials is underpinned by to-pological defects. Given an arbitrary 3D structure from (a) hemispheres to (b) ridges to (c) peaks, the set of topological defect building blocks such as (d) positive and (e) negative disclinations or (f) edge dislocations can be combined to create arbitrary 3D deformation. Engineering topological defects and 3D deformation into 2D materials requires a new degree of control over the spatial arrangement of the defects.

sample can be tuned through a particular arrangement of disclinations and dislocations.

For 2D materials, the basic topological defect that underpins most others is a disclination [47]. A disclination for lattices with 6-fold rotational symmetry like most 2D materials (graphene, h-BN, TMDCs, silicene, phosphorene, etc.) is formed by removing or adding a wedge to change the rotational symmetry to 5-fold (removal) or 7-fold (addition). The symmetry change is readily seen through a Volterra description of the defects as in Fig. 2, where the induced deformation is shown in a continuous medium [48]. In Fig. 2(a,c) positive and negative disclinations are created by tearing the medium, respectively removing or adding a wedge, and restitching it to achieve the configurations in Fig. 2 (b,d). A key challenge to utilizing disclinations for design is that their presence in 2D materials, as compared to bulk materials, is unique. In bulk materials (as well as flat 2D materials), disclinations are essentially non-existent due to their large formation energies arising from the strain field of the rotational defects. However, out of plane relaxation in 2D materials dramatically reduces the in-plane strain and makes isolated disclinations theoretically possible [49]. The out of plane deformation follows the topological character. The positive disclination introduces a 3D deformation with positive Gaussian curvature resembling a hill, while the negative disclination a negative Gaussian curvature resembling a saddle. The absence of disclinations in bulk materials means that there is very little knowledge on how to control or position them.

Edge dislocations, on the other hand, are topological defects that break translational symmetry via the insertion of a half-plane of atoms as shown again using a Volterra description in Fig. 2(e,f). Edge dislocations in 2D materials comprise of a bound positive and negative disclination that share an edge [31]. The introduction of a positive and negative center of curvature in close proximity reduces the strain fields and defect energy. So, while isolated disclinations are not often observed in 2D materials, disclination dipoles (in the form of edge dislocations) are quite common.

Examples illustrating the arrangement of dislocations, and the disclinations that compose them, for a number of 2D materials are reproduced in Fig. 3. Both experimental and theoretical works on flat systems show that oppositely signed disclinations tend to remain bound. In Fig. 3 (a-c), the lattice is assumed to be confined to remain flat, so internal strain is relieved through macroscopic rotation of the grains on either side of the dislocation arrays (grain boundaries). The rotation of the lattice vectors can be clearly seen on either side of the dislocation array

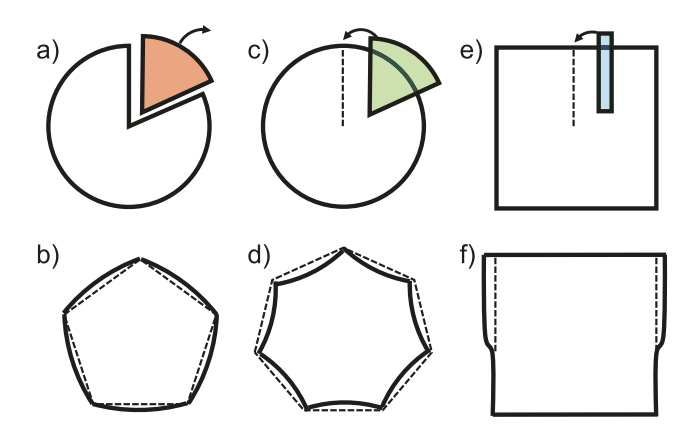


Fig. 2. Volterra definitions of topological defects. (a) Positive disclinations are formed by removing a 60° sector (red) from a triangular lattice. (b) The lattice is restitched to form a five sided shape with convex edges (compare to dotted pentagon). (c,d) Negative disclinations are formed by adding in a 60° sector (green) to a triangular lattice at the dotted line in (c). (d) The deformed structure forms a seven sided shape with concave edges (compare to dotted heptagon). (e) Edge dislocation created by adding a half-plane of atoms (blue) to a lattice at the dotted line. (f) The edge dislocation creates a strain field that creates bulges at the boundary of a sample.

in Fig. 3(b). Experimental observation of topological defects (Fig. 3(d-f)) show that they are not perfectly ordered. Instead, dislocation arrays take on sinuous shapes (Fig. 3(d)), and even positive disclinations with only four atoms have been observed (Fig. 3(f)).

2.2. Usual forward and inverse problem

The 3D deformation associated with a topological defect or distribution of defects can be found through atomic scale (*ab initio* or classical potential) simulations and/or continuum modeling. This corresponds to the *forward* problem: given a defect distribution, find the corresponding 3D structure. Yazyev and Louie first reported 3D deformation from topological defects in 2D materials through *ab initio* calculations of dislocations arrays in graphene [31]. Chen et al. built on this to model the 3D deformation of dislocations using von Kármán equations based on the 3D deformation obtained from atomistic simulations using the classical REBO potential [53]. More recently, Zhang et al. also used the von Kármán equations to model the 3D deformation of isolated disclinations [49].

These atomistic and continuum models obtain the 3D deformation for a given set of topological defects, but the design objective – finding a set of topological defects that results in a desired 3D structure – is better represented via the *inverse* problem. Although the forward calculation of 3D deformations of defect distributions can be input into a search algorithm to find the appropriate one, this approach is more computationally costly than a direct inverse model. The search algorithm would need to optimize both the distribution of topological defects to find a 3D geometry (a non-linear search) allowing for varying the total number of defects present (a grand-canonical optimization problem).

Instead an inverse model may directly solve for the number and type of topological defects necessary to obtain the desired 3D deformation. An example inverse model that utilizes a phase field crystal (PFC) approach was developed by Zhang et al. [7]. The PFC method identifies a possible atomic scale structure by finding the steady state charge density (Fig. 4(b)) on a curved manifold (Fig. 4(a)) [54]. The PFC method is an alternative to molecular dynamics simulations as it simultaneously captures atomic length scales and diffusive time scales. It is governed by the Swift-Hohenberg equation

$$F = \int \left[\frac{\phi}{2} \left(-\epsilon + (1+\Delta)^2 \right) \phi + \frac{1}{4} \phi^4 \right] dx, \tag{1}$$

where Δ is the 2D Laplace operator, ϕ the reduced density, and ε the reduced temperature [55]. If the dynamics are assumed to be dissipative, this amounts to evolving the governing equation

$$\frac{\partial \phi}{\partial t} = \Delta \left\{ \left(- \epsilon + (1 + \Delta)^2 \right) \phi + \phi^3 \right\}$$
 (2)

using a numerical solver such as a finite element method or spectral method. The minima that result from the charge density evolution are converted into a triangular lattice (Fig. 4(c)), the Voronoi tesselation of which is the atomic lattice (Fig. 4(d)).

In Fig. 4(d), isolated disclinations facilitate the 4 nm wavelength of the sinusoidal curvature, but these features have never been observed experimentally and require precise control of defect position and spacing. So, even though this approach finds the atomic structure that corresponds to an arbitrary curved manifold, there is no method to achieving this target distribution of topological defects experimentally. While the inverse approach provides the set of topological defects that underlie a given 3D deformation, achieving the desired set of topological defects is non-trivial. An intimate knowledge of the formation and migration of topological defects is required to achieve the desired configuration.

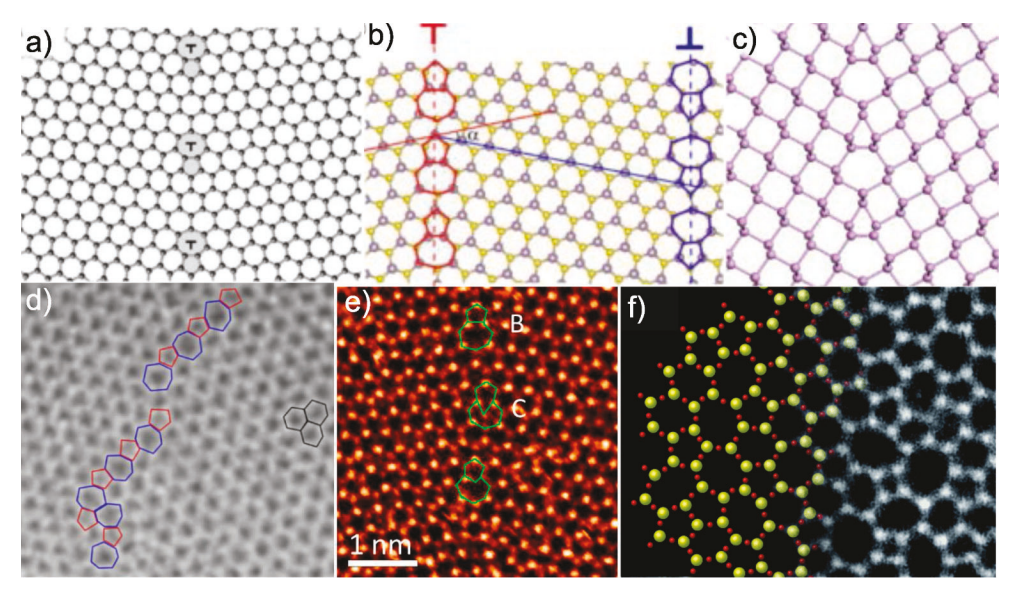


Fig. 3. Examples of topological defects in 2D materials. (a-c) Structural models showing arrays of dislocations composed of positive and negative disclinations in (a) graphene, (b) MoS2, and (c) phosphorene. Reproduced with permission from [47]. (d-f) Transmission electron microscopy images of dislocations in (d) graphene (Reprinted with permission from [50] Copyright 2011 American Chemical Society) (e) MoS2, (Reprinted with permission from [51]. Copyright 2013 American Chemical Society) and (f) silica glass (Reprinted with permission from [52]. Copyright 2012 American Ch.emical Society).

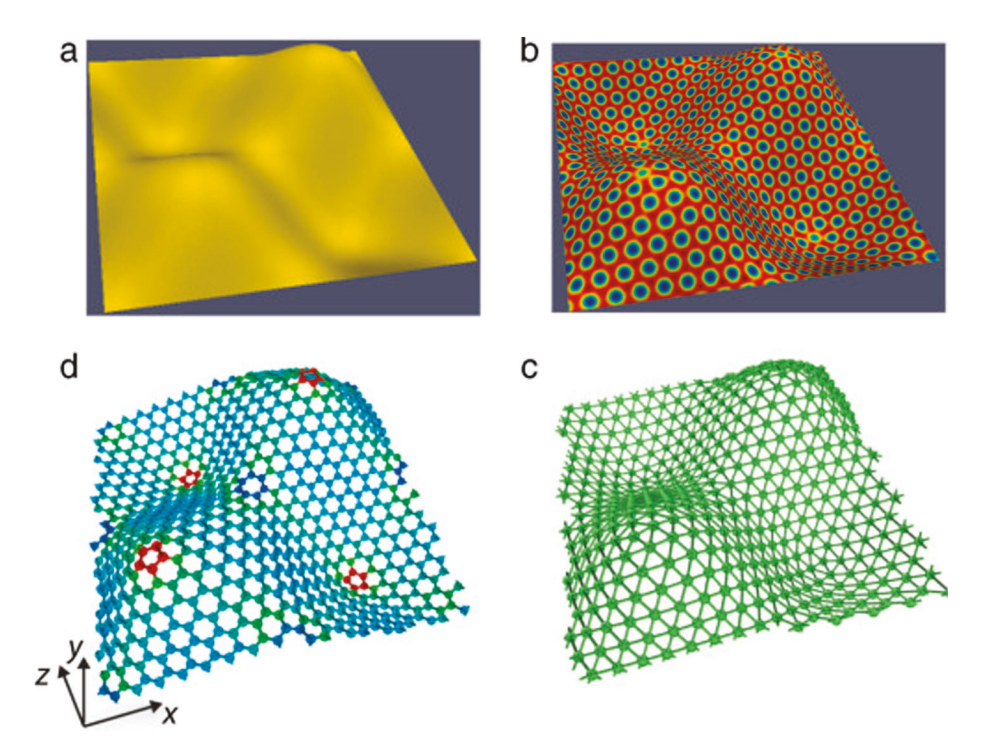


Fig. 4. Overview of inverse design method for topological defects [Reproduced with permission from Ref. [7]]. (a) Input 3D deformation with sinusoidal 3D topology. (b) Charge density map created from the phase field crystal model. (c) Triangular lattice generated from the minima of (b). (d) Voronoi tesselation of the triangular lattice yielding a graphene sample with an array of topological defects.

3. Beyond the forward and inverse problem – tracking the pathways and migrations of topological defects

The forward and inverse problems described above determine the internal strain and 3D configuration for a set of *static* positions of topological defects and *vice versa*. Even given robust solution methods for these, the critical remaining problem lies in their *dynamics* – their motions and migrations, especially in response to applied fields. Given a target spatial distribution, how can defects be introduced in graphene, and then guided in their motions to the target? An understanding of the migration mechanisms and pathways is a prerequisite to answering this question.

3.1. Prior experimental and computational work

Some mechanisms for the formation of topological defects have been identified, but most work has aimed at their observation and not in controlling their movement and position. Experimental observation has shown that topological defects are introduced into 2D materials during synthesis as both geometrically necessary dislocations [56] and as isolated defects [57,58]. For instance, a principal source of topological defects in graphene is grain boundaries, where arrays of dislocations stitch two grains together [59]. The dislocations are geometrically necessary and account for the misorientation between two grains. The specific arrangements of topological defects that can stitch grains together have been enumerated to show the vast arrangements possible

in graphene spanning varying misorientation angles and line directions [60,61].

The large phase space of observed grain boundaries arises from the natural misorientation of 2D materials grown on substrates [62,63]. In addition, during annealing grain boundaries can migrate so as to remove non-equilibrium structures that form during island coalescence during growth, to increase the average grain size. Still, both high and low-angle grain boundaries persist in annealed graphene [64]. While most observed grains are quite large, small grain boundary loops also form resulting in metastable 'flower-defect' configurations [65,66]. The formation mechanisms of flower defects has recently been proposed to be based on a bulge mechanism associated with the dynamic process of annealing [67]. Unfortunately, none of these observations have shown how we can tailor a specific grain boundary structure.

To overcome this, recent theoretical studies have focused on utilizing the substrate morphology to synthesize topological defects directly [30]. However, the substrate topology can only be defined up to a specific resolution set by the limits of lithographic techniques. In addition, nanoscale features tend to become reorganized (e.g. through step bunching) by 2D materials during growth [68,69]. Therefore there remains a need for controlling the position of topological defects.

The control of defect positions is grounded in understanding the topology and mechanisms of dislocation migration. Considering geometry alone, dislocations can be created and manipulated through isolated bond rotations in otherwise pristine material. For example, Stone–Wales defects in graphene form when a single carbon–carbon bond is rotated by 90° , resulting in a 5|7|7|5 quadrupole of disclinations [70,71]. The quadrupole can be thought of as a pair of 5|7,7|5 dislocation dipoles with opposing topological character [72]. Bond rotation is a conservative form of defect introduction since it does not require insertion or removal of atoms. Stone–Wales defects have been observed to form this way in experiment, as a result of electron damage in microscopy

experiments [57,73] or due to ion bombardment [74]. After they are created, the two dislocations present in the Stone–Wales defect could then be separated through additional bond rotations.

In modeling and simulation, the formation and migration of topological defects is most commonly tracked through Monte Carlo (MC) simulations based on bond rotations for conservative glide motion. Recently, climb as well as glide was addressed with a point defect mediated hopping mechanism [77]. Other common approaches such as molecular dynamics (MD) may struggle to capture the long time scales needed, and events such as bond rotations are relatively rare on MD timescales. Early Monte Carlo simulations of carbon nanotubes under constant tensile stress show the role of bond rotations, defect formation, and defect migration in their plastic deformation [78]. Those simulations, for instance, identified a defect unique to 2D systems that could serve as a mediator of plastic deformation known as a 'worm' due to its method of locomotion. Such worms are comprised of alternating arrays of dislocations (a dislocation screened by multiple dislocation dipoles), and form under large applied tensile stress since the screening of the strain fields due to dislocation-dislocation interactions reduces out-ofplane buckling. Other MC simulations address graphitic sp² bonded systems to show the evolution of not only Stone-Wales defects but also more general flower defects and grain boundary loops seen in experiments [79,76]. Most recently, MC approaches have been used to evolve the connectivity of carbon atoms during growth. These simulate the annealing of amorphous carbon to show the origin of defect structures in graphene [75].

Such Monte Carlo approaches are useful, but they require energy calculations at each step to determine the acceptance or rejection of a specific bond rotation. Additionally, within a given instance, pathways are identified for a specific applied load and require a new simulation for each applied load. This becomes computationally expensive as the simulations can require hundreds of thousands of bond rotations. For

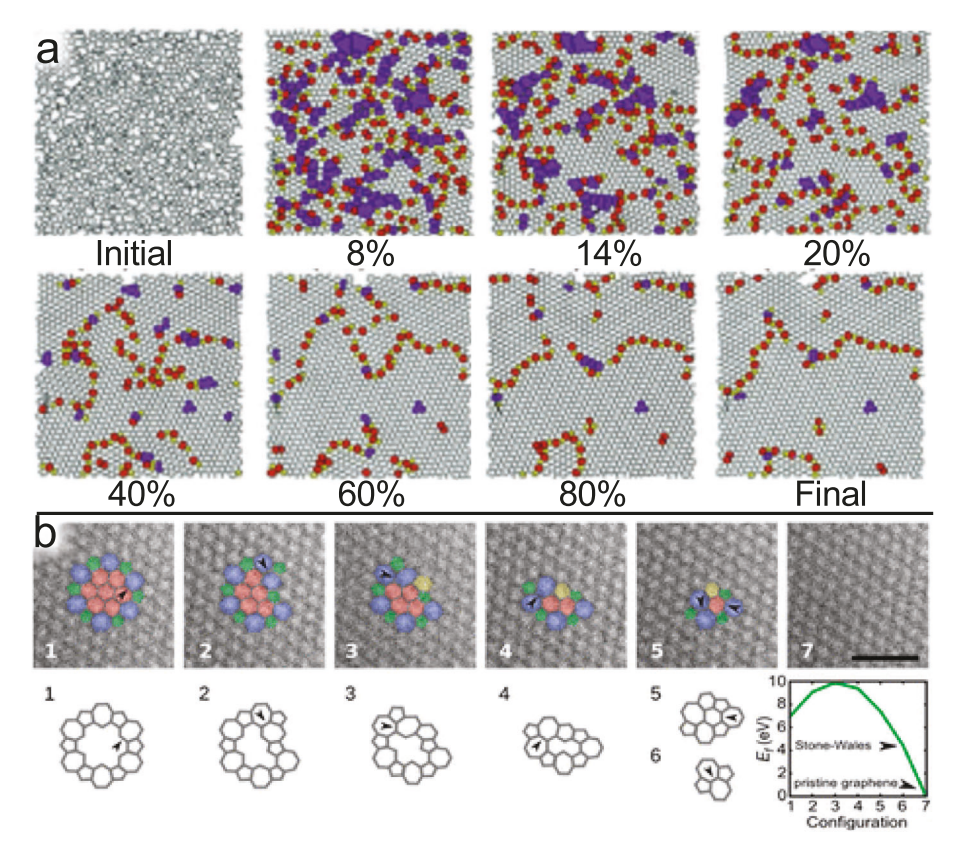


Fig. 5. Examples of Monte Carlo results from prior literature. (a) Formation of graphene from random carbon precursor with bond rotations. Color shows different defect structures in the graphene. Reprinted with permission from [75]. (b) Annealing of a flower defect through bond rotations in both experiment and simulation. Reprinted with permission from [76]). Copyright (2012) American Chemical Society.

instance, in the MC simulation results reproduced in Fig. 5(a), Zhuang et al. simulate a 7.6 nm \times 7.6 nm graphene supercell and, even though 5×10^5 bond rotations are included, the structure still contains features not observed in experiment [75]. Even the evolution of much smaller flower defects carried out by Kurasch et al. in Fig. 5(b) enclose only seven hexagonal rings of carbon but require 5×10^4 bond rotations to recreate the flower topological character [76]. A simple example shows the challenge with MC methods. Given a $100 \times 100 \text{ nm}^2$ sample with 10 dislocations in it that are on average 10 nm from their final position, there are 1052 paths that the dislocations can take to move to their final position. Disclination migration is even more complicated since (as described in the next subsection), it itself is based on dislocation migration. The large computational cost of Monte Carlo methods coupled with their stochastic nature makes it difficult to use them to exhaustively search and identify migration pathways and mechanisms. The phase space of possible pathways is prohibitively large to be fully sampled.

3.2. Example: pathway to create isolated disclinations

To illustrate the challenge in detail, we consider mapping out a single defect migration pathway that yields a specific desired spatial arrangement of topological defects. From this specific example, in the following subsection we will generalize the problem at hand by representing migration pathways as sequences of bond rotations and present a formal statement of the associated *meta* forward and inverse problem.

Our example path is one that leads to the creation of isolated disclinations in graphene. While the formation and migration mechanisms of dislocations (5|7 pairs) is relatively more explored, the formation and migration mechanisms of disclinations (isolated 5 or 7 rings) needs to be further developed. This is especially true since positive and negative disclinations effectively introduce point sources of curvature into a 2D material, and therefore would be effective for designing 3D geometries. The pathway outlined here is one that creates isolated disclinations by taking advantage of the fact that dislocations can be thought of as bound disclination dipoles. It is outlined without regard to its energy land-scape, which we will discuss later.

Fig. 6 shows the hypothetical pathway for creating isolated disclinations using only bond rotations. Starting with pristine graphene in Fig. 6(a), four isolated disclinations are formed in Fig. 6(h). The process is underpinned by dislocation migration, where a 5|7|7|5 disclination

quadrupole is formed in Fig. 6b) and separated through fourteen bond rotations (Fig. 6(c,d)). A second 5|7|7|5 defect forms in Fig. 6(e), and dissociates again (Fig. 6(e,f)). Fig. 6(g) shows the annihilation of disclinations as the negative disclination in one edge dislocation cancels the positive disclination in the other. The annihilation creates four isolated disclinations in Fig. 6(h). In theory, this process can be repeated to form disclination arrays with defined spacing. This path utilizes dislocation migration – described above as a *sequence of bond rotations* – as the basis for positioning disclinations.

However, the path relies only on conservative bond rotations, and is associated with a complex and possibly unattainable energy landscape. Even if this pathway were feasible, it is one of out of many and it is unlikely to be the lowest energy pathway. For instance, the dislocations may migrate through the same worm mechanisms identified in carbon nanotubes or the disclinations could separate into partials connected by a stacking fault [80]. It is not obvious what type of applied loading might help to promote this path. Due to the many different paths that a set of dislocations can take, a more robust approach is needed to enumerate possibilities and efficiently select likely candidates.

3.3. Formal statement of 'meta' forward and inverse problem

To give a formal statement of the *meta* forward and inverse problems, we generalize the example above to consider arbitrary allowable defect migration pathways. A rigorous problem statement helps to define the nature of the search space and conceive solution strategies.

3.3.1. Configuration representation through network connectivity

In principle the presence of topological defects within a hexagonal lattice can be described by the network connectivity of the lattice. In graphene, each atom is bonded to three nearest neighbors to ensure an $\rm sp^2$ hybridization. Some possible connectivities of a graphene sheet are seen in Fig. 7, all showing different arrangements of topological defects preserving $\rm sp^2$ bonding. The black lines in Fig. 7(a) show the connectivity for pristine hexagonal graphene, with points (atoms) labeled by letters. In the pristine configuration C_i each atom is linked to three others, as enumerated in Table 1 and the configuration energy is E_i . Connected points are listed in a clockwise sense around the central point. (see Table 2).

If a single bond rotates by 90° degrees, the connectivity of the network changes but maintains sp^2 bonding. The topological

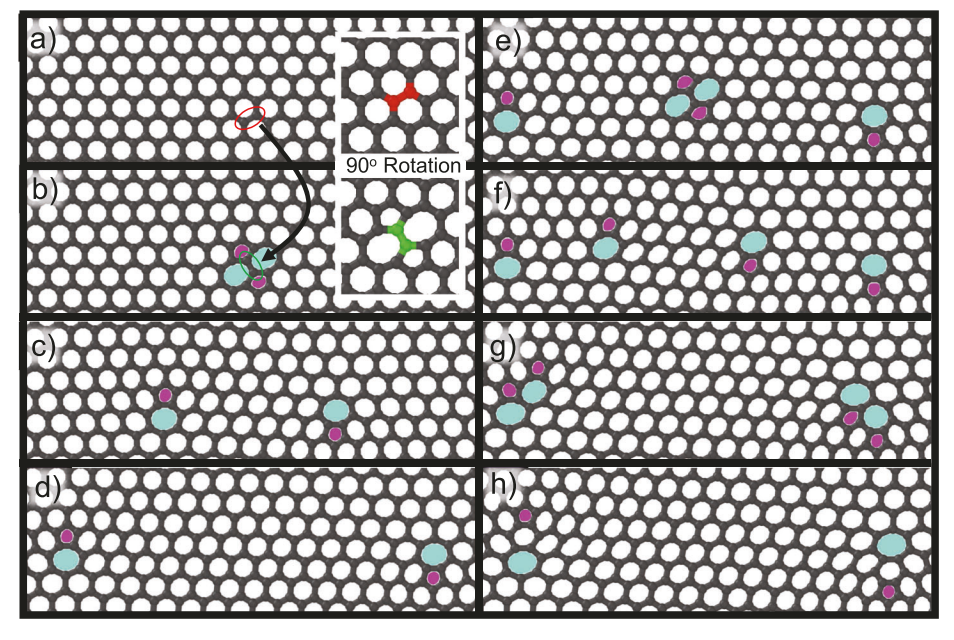


Fig. 6. Mechanism for forming and migrating disclinations. (a) Starting with pristine graphene, a 5|7| 7|5 defect is formed in (b) through a bond rotation (inset b,c). (c,d) Bond rotations create isolated edge dislocation (5|7,7|5) with a desired spacing. (d) A second 5|7|7|5 defect is formed one lattice vector above the first one in (b). (f,g) Bond rotations create isolated edge dislocation (5|7,7|5) up until the same sign dislocations are sharing carbon atoms. (h) The same sign dislocations react to create isolated disclinations separated by a hexagonal ring. Color coding is used to highlight positive (magenta) and negative (cyan) disclinations.

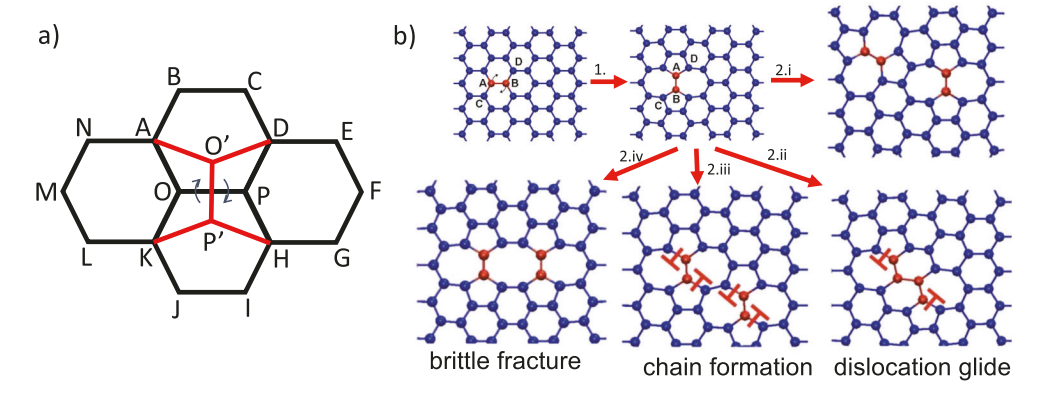


Fig. 7. Definition of network connectivity for graphene. (a) The connectivity between atoms (points) are the three bonds (lines) that connect them to adjacent atoms. A 90° rotation of bond OP to O'P' changes the network connectivity to the lines in red. (b) The network connectivity is altered by successive bond rotations. From a 5|7|7|5 defect the connectivity diverges and requires accounting for a particular sequence of configurations.

Table 1 Network connectivity table for the configuration shown in Fig. 7(a). Points are labeled by letters, and for sp^2 bonding each point is connected to three neighbors for a given configuration. Configuration C_i describes the neighbors around each point before bond rotation (black) while configuration C_{i+1} shows a configuration accessible from C_i via a single bond rotation.)

Pt.	C_i	\rightarrow	C_{i+1}
D:	$\{P,C,E\}$	\rightarrow	$\{O,C,E\}$
K:	$\{L,O,J\}$	\rightarrow	$\{L,P,J\}$
O:	$\{A,P,K\}$	\rightarrow	$\{A,D,P\}$
P:	$\{O,D,H\}$	\rightarrow	$\{O,H,K\}$

Table 2 A collection of paths S_j that evolve the initial connectivity $C_{j,0}$ to show the divergence of paths in 7 (b). Each path has an index j that is associated with each connectivity $C_{j,i}$.

S ₀ :	$\{C_{0,0},C_{0,1},C_{0,2i},\ldots\}$
S_1 :	$\{C_{1,0},C_{1,1},C_{1,2ii},\ldots\}$
S_2 :	$\{C_{2,0}, C_{2,1}, C_{2,2iii}, \ldots\}$
S_3 :	$\{C_{3,0},C_{3,1},C_{3,2i\nu},\dots\}$

rearrangement for rotation of bond OP is shown in red in Fig. 7a) and introduces a 5|7|7|5 quadrupole of disclinations. The bond rotation involves changes to the connectivity of four atoms (D, K, O, P). The change in connectivity is shown in Table 1: points O,P swap neighbors K,D and points K,D swap neighbors O,P.

The set of all possible configurations C that maintain sp^2 connectivity is an equivalence class. Each possible defect arrangement corresponds to a configuration C: the topology of each dislocation configuration is unique and can be described by its connectivity. The usual forward problem can be posed as: given a network configuration C, what is the associated 3D structure? And the usual inverse problem can be posed as: given a desired 3D structure, what is the needed network configuration?

3.3.2. Defect migration pathways as sequences of bond rotations

 ...} with associated configuration energies $\{E_0, E_1, E_2, ...\}$. For example, the Stone–Wales bond rotation described in Fig. 7(a) updates the connectivity from configuration C_i with energy E_i to C_{i+1} with energy E_{i+1} , where the latter is accessible from the former through the bond rotation. A particular pathway S consists of sequences of configurations where C_{i+1} is accessible from C_i because the connectivities differ by only a single bond rotation.

Starting at an initial connectivity C_0 the superset $S = \{S_1, S_2, S_3, ...\}$ lists the unique paths $S_j = \{C_{j,0}, C_{j,1}, ...\}$ that are possible. For instance, in Fig. 7(b) the sample starts with connectivity C_0 and with a bond rotation transforms to C_1 , introducing a Stone–Wales defect according to the rules from Fig. 7(a). A subsequent bond rotation can annihilate the original Stone–Wales defect, create an additional Stone–Wales defect C_{2i} , create an octagon C_{2ii} (typically leading to strain localization and brittle failure), form a chain C_{2ii} , or advance an existing dislocation by one Burger's vector C_{2iv} (glide). To find the corresponding configuration energies, the atomic configuration of each candidate state should be optimized subject to the constraint that its network topology is fixed. In this way, local minima of the potential energy surface (PES) are sampled.

Such enumeration of pathways, where allowable configuration changes can be considered systematically in terms of accessible modifications to ring connectivity tables, enables a degree of organization within the large phase space of pathways. Elements S_j of $\mathbb S$ take on a tree structure that branches outwards starting from a fixed initial configuration. The pathways described this way will exhibit large diversity, and path enumeration like this could be extended to 2D materials beyond graphene with slight modification. For example, the formation of 3-fold rotational 'trefoil' defects (8–4-8–4 rings with trigonal symmetry) in boron nitride when isolated vacancies cluster together involves one 60° rotation of three atoms neighboring another [81]. The formation of mirror twin boundaries in MoSe₂ when Se vacancies coalesce [82] requires a sequential set of bond rotations similar to formation of 'worms'.

The superset $S = \{S_j\}$, $j = 1, 2, 3, \dots$ defines the phase space of paths from an initial position, capturing in full the divergence of paths from an initial configuration C_0 . The *meta* forward problem then becomes efficiently selecting the most likely sequence S amongst all elements of S, given the initial configuration and the application of a prescribed load. The *meta* inverse problem is to find what mechanical loading to apply, if a given path is desired. The *meta* forward problem requires an efficient approach to identifying candidate pathways and determining their energy landscape. The *meta* inverse problem requires a way to efficiently search the set of all possible sequences and select the viable ones in a given setting/environment.

4. Predicting applied load to control topological defects

Realizing a specific distribution of topological defects to create a desired deformation will enable designing the 3D deformation of 2D materials. Achieving this control requires understanding defect mechanisms of migration, especially in response to applied loads. Here we briefly review how applied loads induce forces on topological defects; we show an illustrative example of how a displacement boundary condition (given as an applied strain) can alter the energy landscape of defect migration; and we discuss opportunities to address the meta forward and inverse problems that determine the path of topological defects in response to an applied load, and the load that gives a desired migration path for topological defects.

4.1. Forces on dislocations arising from external fields

Externally applied loads and body forces induce configurational forces on topological defects, which is the basis for guiding their motions along a desired path. Specifically, external loads can be applied in the form of traction and/or displacement boundary conditions that induce a particular stress, strain, and displacement state in a boundary value problem. When present, these external fields interact with the corresponding internal fields of the defects. The interaction reflects the fact that the minimum energy configuration (spatial distribution) of a set of topological defects in the presence of an external field is generally not the same as the minimum energy configuration in the absence of the external field. As a result, the introduction of an external stress may cause defects to move, inducing a rearrangement.

The tendency of a dislocation to move through the crystal in response to an stress field is described by the Peach-Koehler (PK) force:

$$f_n = \sigma_{ij} n_j b_i, \tag{3}$$

where the force f_n is the result of the external stress σ_{ij} acting on a dislocation that moves on plane with unit normal n_j and dislocation Burgers vector b_i [83]. The force on the dislocation is based on its topological character, *i.e.* the Burgers vector. It is therefore a result of the lattice incompatibility. The plane on which the dislocation moves depends upon whether the motion is in the form of climb, glide, or cross slip. This configurational force on the dislocation provides a means of controlling it. Since the topological content of disclinations can be modeled as an array of dislocations [84], the force on disclinations can be found through the PK force on all the constituent dislocations. Alternatively, numerical methods that find the energy of disclinations

can be used to solve for the force as shown by Zhang et al. [49].

4.2. Example: Using strain to control dislocation spacing

The forces on dislocations, and the associated potential energy landscape, can be used to induce a desired migration pathway amongst dislocations. Here we return to our previous example, and show how the application of an external shear (e.g. via fixed displacement boundary conditions) can affect the energy landscape of the pathway shown in Fig. 6 where dislocation dipole separation results in the formation of isolated disclinations. The geometry of the supercell, the shear ε_{xy} applied to it, and resulting change in geometry, is shown in Fig. 8(a). The shear is applied in a direction perpendicular to the line along which the dislocation dipole separates. The curves in Fig. 8(b,c) show the local minimum energies for each network connectivity shown in Fig. 6, thereby mapping out the potential energy surface (PES) along the path. They are determined assuming that the graphene sheet is constrained to remain flat along the entire pathway. The family of curves presented in Fig. 8(b,c) corresponds respectively to the introduction and separation of the first and second set of dislocation dipoles, respectively. The energies are calculated using LAMMPS [85] with the interatomic potential AIREBO [86].

Fig. 8(b) shows the energy landscape to introduce and dissociate the first dislocation dipole (d_1) , for varying external applied shear. The applied strain field changes the potential energy surface such that dislocation dissociation becomes favorable and makes 5|7|7|5 dipole separation possible. As shear strain is applied, the energy landscape for dislocation separation is altered to create a meta-stable 5|7|7|5 dislocation configuration that is separated. As the applied shear increases, the dislocation separation that minimizes the total energy becomes larger, as shown by the black dotted line. The minimum in the energy corresponds to the configuration where the PK force is zero. If larger shear is applied (not shown), the initial thermodynamic barrier (spacing $d_1 = 1$ nm Fig. 8(b)) is overcome at 3.5% strain, removing the effective barrier to dipole separation. Of course, the simple picture for the separation of a single dislocation dipole would be more complicated than shown if a more complex topological structure (like a larger number of pre-existing defects) were present. For example, the potential energy surface associated with grain boundary migration contains numerous metastable configurations of dislocation arrays [87].

Fig. 8(c) then shows the energy landscape associated with introducing and dissociating the second dislocation dipole. This pathway corresponds to the bond rotations shown in Fig. 6(e-h), the end result of

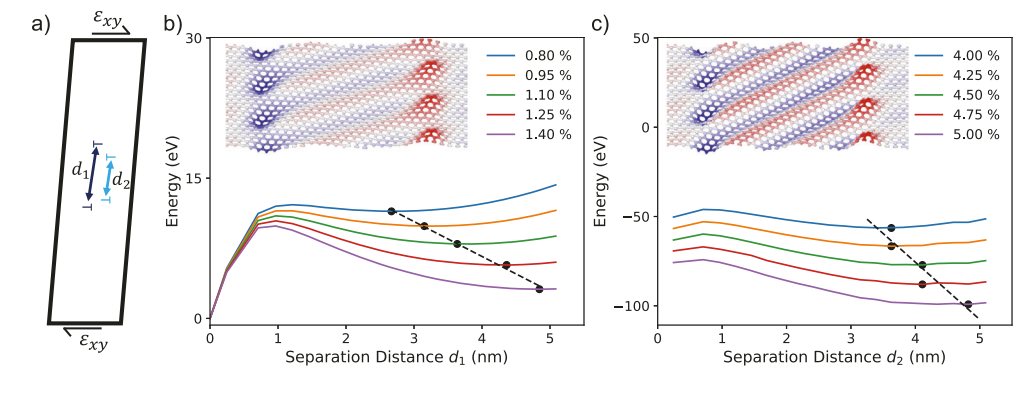


Fig. 8. Dislocation separation versus energy from a 5|7|7|5 defect for flat bilayer graphene. (a) Schematic of the dislocation geometry, where a shear strain ε_{xy} is applied at the boundary of a periodic unit cell, and dipoles with separation d_1 and d_2 . (b) Energy versus separation d_1 of a single dipole (d_2 = 0) for various applied shear strains, where 0 nm spacing contains no defects. (c) Energy versus separation d_2 for a second dipole $(d_1 = 5 \text{ nm})$ for various applied shear strains, where the zero energy reference is the same as (b). Dotted lines in (b,c) connect minima in the potential energy and reveal how to tune the dislocation spacing. Insets in (b,c) correspond to three unit cells with 5 nm spacing between topological defects after strain has been released to allow 3D deformation. Inset color goes from -3 nm (blue) to 0 nm (white) to 3 nm (red). (For interpretation of the references to colour in this figure legend, the reader is referred to the web version of this article.)

which are isolated disclinations. From Fig. 8(a), we simulate the separation d_2 of the light blue dislocations as the dark blue dislocations are fixed with separation of $d_1 = 5$ nm. In Fig. 8(c), the minimum energy separation of the second dislocation dipole is altered by the external strain in the same way as a single dipole. A key difference is the higher external strain field needed, which results from the need to overcome the strain field of the first set of dislocations itself.

Once the dislocations have been positioned as desired, the external strain field can be relieved and the graphene sheet released from the substrate. The 2D material can deform out of plane, revealing the spontaneous 3D deformation (insets in Fig. 8(b,c)) induced by the array of topological defects. Even in these simple examples, the difference between the 3D structure of bound vs. separated disclinations shows how precisely topological defects alter 3D deformation. The 3D deformation in the inset in Fig. 8(b) is largely localized to the dislocations, whereas the 3D deformation in the inset of Fig. 8(c) shows ridges spanning the entire 5 nm separation, with a peak-to-peak amplitude of 6 nm and wavelength of 1.3 nm.

These two contrived examples illustrate the concept of using strain to control dislocation position. However, the dimension of the potential energy surface increases rapidly when more than dislocation dipoles are considered. In addition to creating dislocations through 5|7|7|5 defect formation and separation, as-grown dislocations can be utilized from nanograined 2D materials, where strain could be used to manipulate the densely packed grain boundaries through shear coupling [88,89]. However, the more dislocations that are present the more complex and high-dimensional the energy pathways become (as described in Section 3.3.2). To address the more complicated scenario of multiple topological defects and branching paths, we explore automated methods for determining the evolution of defect spatial distribution given a more complex potential energy surface.

4.3. Forward problem: finding the path for a prescribed load

Finding the path a topological defect follows in the presence of a prescribed loading constitutes the meta forward problem. The system parameters - material, applied fields, and initial configuration - are defined and the topology is evolved to obtain the path and final configuration. While this problem is challenging due to the large dimension of the search space, any solution strategy must involve first mapping the potential energy surface to identify the low energy valleys, and then using the mapping to identify the path along which the network topology changes. This approach to the forward problem is shown in Fig. 9, and also serves as the basis for any attempt at inverting the solution.

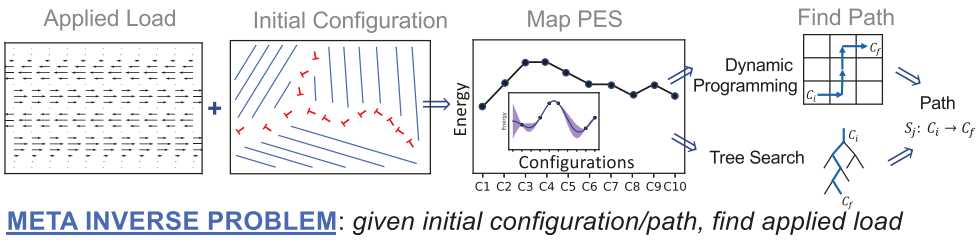
4.3.1. Mapping the potential energy surface

Mapping the PES, and therefore navigating the space of configurations, is challenging due to the many energy evaluations needed to approximate the smooth variation of energy in a high dimensional space. While the energy of every possible configuration could be estimated – using atomistic methods, continuum methods, or a combination - this is extremely inefficient since most configurations are not realistic and since relationships exist between the energies of adjacent states. Such relationships are evident in Fig. 8(b,c), where each energy trajectory could be described by the interaction energy of the dislocations and the elastic strain in the supercell. Instead, an approach that efficiently identifies and maps the low energy pockets of the configuration space, and avoids the unreasonably high energy portions, is desirable.

The most commonly used approach to identify relevant configurations is to map the high dimensional PES using Monte Carlo methods to find minima [90]. When using Monte Carlo approaches, the PES is sampled along a chain of connected states (evolved by, e.g., bond rotations). However, the effectiveness of the MC search through high dimensional space is limited. For example, when mapping a PES via bond rotations, from a given configuration typically one considers all possible bond rotations determines the energy change despite that most bond rotations are unlikely or irrelevant. Assuming that a computational engine is available that can robustly and efficiently return the energy when presented with a given configuration, then improvements over Monte Carlo may be possible.

For instance, in terms of more efficient strategies, there is an opportunity in new machine learning methods like probabilistic Gaussian process models. Gaussian process models can take into account the correlations in the PES and can both map the PES and give estimates on the uncertainties in the mapping. In a Gaussian process model, numerous random samples of the entire potential energy surface are generated, which enables identifying the dominant low-energy pockets and assigning uncertainties to the unexplored regions. The uncertainties direct the PES exploration such that not only are the minima discovered but the entire PES can be approximated within a desired tolerance [91,92]. A simplified demonstration problem could be defined in which the PES that spans between two prescribed local minima is searched and mapped. When calculating the energy of the system, any of the methods introduced in Section 2.2 including ab initio, classical potentials, or continuum modeling can be used. In fact, a number of these could be combined with the error estimation to form high, medium, and low fidelity models that reduce the variance associated with the Gaussian

META FORWARD PROBLEM: given applied load/initial configuration, identify path



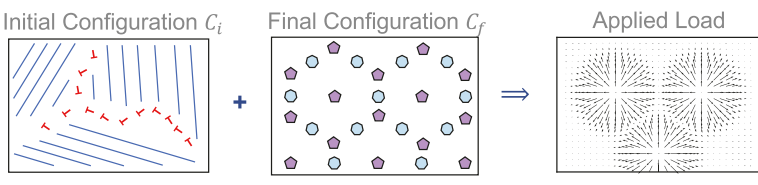


Fig. 9. Methods of Meta Forward and Inverse Problems. The meta forward problem identifies the path S_i of topological defects from an initial configuration for a given applied field. The path is found by mapping the potential energy surface and then identifying a path. The meta inverse problem identifies the applied load that transforms an initial to final connectivity.

process model [93].

4.3.2. Finding the path through a PES

Navigating a high-dimensional network topology according to the potential energy surface is challenging due to the non-locality of the problem. Changing one bond rotation in the path will affect every subsequent bond rotation. However, there are many well-established methods that determine migration paths through a potential energy surface, once the potential energy surface is known [94]. Although here we address the migration of topological defects, the problem of finding paths through potential energy surfaces is quite broad and applies to many physical questions including ion diffusion and annealing. Paths can be identified based on several criteria, for example:

- Minimize final configuration energy: Identifying the path that gives the
 largest total reduction of energy between the initial and final
 configuration. Note that this would not require explicit knowledge of
 the path, but only its initial and final configuration, and therefore
 more closely resembles the original forward and inverse problem.
- Steepest descent: Identifying the path that gives the largest total reduction of energy possible at each step.
- Minimize largest energy increase between two successive configurations: Given sequence energies $\{E_{j,0}, E_{j,1}, E_{j,2}, ...\}$ for path S_j , the largest energy change is given by $\Delta E_j = \max_i (E_{j,i+1} E_{j,i})$. The selected path S_j is then the one that has the smallest ΔE_j .
- Minimize largest energy increase between two configurations: Given sequence energies $\{E_{j,0}, E_{j,1}, E_{j,2}, ...\}$ for path S_j , the largest energy change is given by $\Delta E_j = \max_i (E_{j,i'} E_{j,i})$ where i' > i. The selected path S_j is then the one that has the smallest ΔE_j . That is, avoid paths that traverse steady climbs over the potential energy landscape over several steps.

Since the energies considered are local minima of metastable states of the PES, further complexity could be introduced by considering transition states between successive configurations [95,96]. The metrics are useful for evaluating the likely path through a PES. Coupled with the enumeration of paths given in Section 3.3.2, these criteria allow for a ranking system of what the most likely paths are.

The problem of mapping the PES and finding an optimal path through it could be merged by combining Gaussian process modeling and dynamic programming. In fact, this approach has recently been demonstrated to predict transport pathways for proton diffusion in oxides [97]. As a demonstration, one could search a path between two well-defined local minima in the PES based on the criterion that the energy barrier along the path be minimized. A Gaussian process model could be used to iteratively update the description of the PES, based on the estimated uncertainty of the energy barrier itself. Dynamic programming is an optimization method that can be applied to simplify a complex search by recursively breaking it down into simpler subsearches. Dynamic programming algorithms have been shown to be effective at finding paths through PES [97,98], and may be effective for searching through the lattice network space here as well. Additionally this approach offers the advantage that it does not rely on prior knowledge, and therefore may not be biased by preconceptions of likely pathways.

Alternatively, given the tree-like structure of the space of migration paths, the optimal path might be determined using Monte Carlo Tree Search (MCTS) algorithms [99,100]. MCTS excels in scenarios where the number of choices in successive branches becomes too computationally expensive to calculate exhaustively, and underpins recent accomplishments of AI in the games of chess or GO [101]. In addition, MCTS has been applied to materials informatics. It has mainly been used in the space of molecular chemistry to discover new molecules and to determine how to synthesize them [102–104]. The principal underlying MCTS is to assess the most promising move (bond rotation), where the

search space is expanded by random sampling of possible sequences. It is applied by generating multiple *play-outs*, where a game is 'played out' to the end by selecting moves randomly. The final outcome of each play-out – in our case a sequence of bond rotations – would be weighted by a given metric – in our case the energy barrier – so that better choices are made in forthcoming rounds. A similarity between AlphaGO and the physical applications of MCTS are that the decision making can be accomplished by a neural network (NN). The deep learning method allows for efficient exploration in the network structure [105]. The metrics for suitable paths can be used to define the loss function of a NN that is able to optimize the local choices that are made using previous knowledge of simulation results. In comparison to dynamic programming that only uses the metrics, the NN is able to determine its own heuristics to make decisions in order to gain the same desired outcome.

Together, path selection metrics together with robust approaches to PES mapping and path finding are critical to solving the *meta* forward problem. However, what we are after is the inverse, determining an applied field that produces a desired set of topological defects. We next show how the forward problem is necessary in order to formulate a strategy for the inverse problem.

4.4. Inverse problem: finding the load to control topological defects

The *meta* inverse problem is to identify what field to apply to achieve a target configuration from a prescribed initial configuration. For instance, in Fig. 9 the initial configuration C_i , three grain boundaries (arrays of dislocations \bot), and final configuration C_f , an array of disclinations, are given as the inputs to the inverse model. The inverse model aims to find the loading that results in a path that corresponds to the configuration transformation $C_i \rightarrow C_f$. The specific path that connects the initial and final configurations is not as important as the final configuration. The degree of freedom in the path allows for putting constraints on the applied load such that it can be accomplished experimentally.

Here we suggest two strategies to the inverse problem. The first is a conventional approach that utilizes the forward method to iteratively find an applied load that produces a path that gives the final configuration. The second is based on supervised machine learning, which uses the conventional approach to generate labelled data and identify correlations in the data. For instance, a loading that is applied to a material to control the path does not change the path $\{C_0, C_1, C_2, \ldots\}$ but does change the potential energy surface $\{E_0, E_1, E_2, \ldots\}$ the path traverses. In Fig. 8, the same path is taken in each instance, but different applied loads change the potential energy surface that dictates a particular dislocation separation. The second approach has been shown to be effective in finding predictive inverse solutions and can more directly find the applied load [106,107].

4.4.1. Iteratively finding the optimum loading

The conventional approach is based on updating the applied loading until a path that produces the desired final configuration is achieved. An initial guess of the applied load would be provided, and the forward solution used to find the path and final configuration. Optimization of the applied load would be based on minimizing the distance of the predicted to the desired final configuration. In addition to this primary metric, a number of others may prove useful to optimizing the load. One such metric, for example, is the distance of the closest point in the predicted path to the final configuration. A configuration in the path generated by the forward solution may be closer than the predicted final configuration or even contain the desired final configuration. So, instead of finding a better end point, the algorithm may be able to update the applied load to terminate the path after fewer bond rotations. Additional considerations would be to include metrics that account for the feasibility of applying the particular load experimentally, or checking the sensitivity of the path to the applied load to make it more robust in light of experimental uncertainty.

Optimizing the load is a highly non-linear problem as small changes could change the path dramatically by making a new path suddenly accessible [97]. Therefore, while a gradient descent algorithm could be used to find solutions that are close, it may have a hard time exploring the phase space effectively. Instead, genetic/evolutionary algorithms that sample the phase space and build solutions iteratively may be effective to find the applied loading [108]. A possible merit to the use of genetic algorithms is that the spatial distribution of the applied load can be mapped to the fitness of the resulting path such that genetic representations of the effective regions of the loading field are passed on through cross-over but ineffective areas are blended to explore new areas of phase space.

4.4.2. Direct calculation of the applied load through deep learning

The conventional solution to the inverse problem is reliable but not efficient at solving for the applied load since iterative search is needed. Instead, a deep learning model may be able to find correlations in the data generated by the conventional approach that can produce an applied load directly from the network topology and the initial and final configurations. This is a typical use-case of supervised machine learning models, where although physical solutions to the problem may exist, the solution may be computationally expensive or require a sufficient amount of human input. In this case, the challenges posed may warrant developing a machine learning model.

The concept of network connectivity as described in Section 3.2 has recently been used to predict the stability of inorganic crystals [109-111]. The approach uses convolution layers to transform a graph representation of a material to a vector and finally to produce an estimate of the formation energy (or some other quantity) as an output. A convolutional neural network (CNN) is a class of deep neural networks that is commonly applied to analysis of visual representations of systems. In addition to the graph convolution, the deep learning approach requires utilization of contextualization techniques to map an entire loading field instead of a single output. Insight may be gained from a recent 'U-Net' architecture that provides context to the output to produce a field instead of a single value [112] U-Net is able to generate a pixel-by-pixel map of the output field (applied load) using the inputted information (desired 3D configuration), wherein concatenation in the 'U'-shaped architecture gives the context for the features. The approach has been shown to work well in computer vision and does not require large amounts of training data to produce accurate results [113]. Combined, the graph and U-Net architectures facilitate the input of network topologies in the form of graphs and output a spatially resolved loading condition. The model would be fit with data generated from the conventional approach.

The load, in addition to being the solution to the inverse problem, can be input back into the forward solution to find the actual path that topological defects follow. The paths themselves may yield insight into defect migration mechanisms. Broadly, the trends can be separated into either random or sequential migration, where sequential migration is based on individual topological defects moving directly from their final to initial configurations as seen in Fig. 7. In reality, the migration will be a blend of sequential and random migration. Here, unsupervised clustering of network topologies may illuminate the concerted migration of dislocations that occurs within a path.

5. Experimental linkage

A major driver of this work is to show what is needed in order to realize the potential of controlled atomic-scale 3D deformation of 2D materials. Success though ultimately hinges on linking the theoretical predictions of atomic scale 3D deformation to experimental capabilities and realization of prediction. The path we have detailed addresses the missing theoretical techniques that link the set of topological defects that have been predicted to yield a desired 3D deformation to applied,

experimentally achievable loads that control the formation and migration of topological defects.

It will be critical to utilize experimental observation to develop the theoretical techniques. A preliminary testing area is the annealing of grain boundary loops created during synthesis. For this test case, the migration of dislocations can be observed without any applied load, where the boundary conditions are relaxed due to high annealing temperatures. The migration can be observed in situ as has recently been done for graphene grain boundary migration [114,115]. These observations, where there is no applied load, serve as a good stepping stone as they do not require new experimental techniques or specialized manipulation.

As the dislocation migration mechanisms are validated without applied load, they can be extended to actively control topological defect distribution with applied load. For example, load can be applied to a sample using hydrostatic pressure, voltage, or even mechanical contact. Applying strain to 2D materials is often accomplished through drumhead devices, where pressure, voltage, and contact can impart biaxial strains onto a sample [1,116-118]. Local control of the strain distribution could be accomplished through patterned substrates like nanopillars and nano-spheres [119,120,4]. In addition, mechanical contact can be made through tip based methods that locally deform a sample [121,122]. Each of these methods alters the applied strain in a 2D material due to the particular loading condition of the experimental setup. An important aspect of the experimental verification will be to correctly translate manipulation methods to the loads that they apply. Microscopy techniques that can map the strain with high accuracy without damaging the samples will be critical to ensuring this [123]. Finally, the experimentally achievable loads will have to be used to bias the computational techniques such that the predicted loads are experimentally achievable.

6. Conclusion

Atomic scale control of 3D deformation in 2D materials presents great opportunity, but viable means of control remain elusive to date. Here we have presented a survey of recent findings that facilitate control of 3D deformation at the nanoscale using topological defects. We suggest that control of the positions and spatial distributions of topological defects - in particular - is a key to achieving atomic scale control. In addition, we have identified gaps between simulation and experiments and proposed the computational tools that may help to close that gap. From the computational perspective, progress can be made by developing detailed understanding of the formation and migration mechanisms of topological defects. We describe new meta forward and inverse problems that will be key to establishing how to use external applied loads to achieve a desired spatial distribution of defects. Possible routes to these problems based on emerging numerical methods, machine learning, and deep learning, are outlined. These steps pave the way for experimental work that can further increase the validity of these methods by adding experimental pathways into the loading prediction from the neural network. Ultimately, we believe that these steps will facilitate the development of novel control of 3D deformations at atomic length scales.

Declaration of Competing Interest

The authors declare that they have no known competing financial interests or personal relationships that could have appeared to influence the work reported in this paper.

Acknowledgements

EA and EE acknowledge support through the National Science Foundation under Grants No. DMR-1555278 and DMR-1720633. EA and HJ also acknowledge support through ARO Grant No. ARMY W911NF-

17-1-0544

References

- C. Lee, X. Wei, J.W. Kysar, J. Hone, Measurement of the elastic properties and intrinsic strength of monolayer graphene, Science 321 (5887) (2008) 385–388.
- [2] Q. Lu, M. Arroyo, R. Huang, Elastic bending modulus of monolayer graphene, J. Phys. D: Appl. Phys. 42 (2009) 102002.
- [3] Y. Wei, B. Wang, J. Wu, R. Yang, M.L. Dunn, Bending rigidity and gaussian bending stiffness of single-layered graphene, Nano Lett. 13 (2013) 26–30.
- [4] Y. Zhang, M. Heiranian, B. Janicek, Z. Budrikis, S. Zapperi, P.Y. Huang, H. T. Johnson, N.R. Aluru, J.W. Lyding, N. Mason, Strain modulation of graphene by nanoscale substrate curvatures: A molecular view, Nano Lett. 18 (2018) 2098–2104.
- [5] Z. Li, Y. Lv, L. Ren, J. Li, L. Kong, Y. Zeng, Q. Tao, R. Wu, H. Ma, B. Zhao, D. Wang, W. Dang, K. Chen, L. Liao, X. Duan, X. Duan, Y. Liu, Efficient strain modulation of 2d materials via polymer encapsulation, Nat. Commun. 11 (2020) 1151.
- [6] P. Jia, W. Chen, J. Qiao, M. Zhang, X. Zheng, Z. Xue, R. Liang, C. Tian, L. He, Z. Di, X. Wang, Programmable graphene nanobubbles with three-fold symmetric pseudo-magnetic fields, Nat. Commun. 10 (Jul 2019) 3127.
- [7] T. Zhang, X. Li, H. Gao, Designing graphene structures with controlled distributions of topological defects: A case study of toughness enhancement in graphene ruga, Extreme Mech. Lett. 1 (2014) 3–8.
- [8] N.W. Karuri, S. Liliensiek, A.I. Teixeira, G. Abrams, S. Campbell, P.F. Nealey, C. J. Murphy, Biological length scale topography enhances cell-substratum adhesion of human corneal epithelial cells, J. Cell Sci. 117 (15) (2004) 3153–3164.
- [9] E.K. Yim, K.W. Leong, "Significance of synthetic nanostructures in dictating cellular response,", Nanomed.: Nanotechnol. Biol. Med. 1 (1) (2005) 10–21.
- [10] Y. Yang, K.W. Leong, Nanoscale surfacing for regenerative medicine, WIREs Nanomed. Nanobiotechnol. 2 (5) (2010) 478–495.
- [11] M. Kothari, M.-H. Cha, K.-S. Kim, Critical curvature localization in graphene. i. quantum-flexoelectricity effect, Proc. Roy. Soc. A: Math., Phys. Eng. Sci. 474 (2214) (2018) 20180054.
- [12] M. Diab, T. Zhang, R. Zhao, H. Gao, K.-S. Kim, ruga mechanics of creasing: from instantaneous to setback creases, Proc. Roy. Soc. A: Math., Phys. Eng. Sci. 469 (2157) (2013) 20120753.
- [13] M. Kim, S. Kim, S. Im, Wrinkling behavior of bilayer graphene sheets bonded to an elastic foundation, Int. J. Solids Struct. 178–179 (2019) 36–47.
- [14] M.S. Bronsgeest, N. Bendiab, S. Mathur, A. Kimouche, H.T. Johnson, J. Coraux, P. Pochet, Strain relaxation in cvd graphene: Wrinkling with shear lag, Nano Lett. 15 (2015) 5098–5104.
- [15] J. Kim, J. Leen, H.N. Kim, P. Kang, J. Choi, M.F. Haque, D. Kang, S. Nam, Uniaxially crumpled graphene as a platform for guided myotube formation, Microsyst. Nanoeng. 5 (2019) 53.
- [16] D. Rhee, J.T. Paci, S. Deng, W.-K. Lee, G.C. Schatz, T.W. Odom, Soft skin layers enable area-specific, multiscale graphene wrinkles with switchable orientations, ACS Nano 14 (2020) 166–174.
- [17] M.C. Wang, J. Leem, P. Kang, J. Choi, P. Knapp, K. Yong, S. Nam, Mechanical instability driven self-assembly and architecturing of 2d materials, 2D Mater. 4 (2017) 022002.
- [18] S. Deng, V. Berry, Wrinkled, rippled and crumpled graphene: an overview of formation mechanism, electronic properties, and applications, Mater. Today 19 (4) (2016) 197–212.
- [19] J. Yu, S. Kim, E. Ertekin, A.M. van der Zande, Material-dependent evolution of mechanical folding instabilities in two-dimensional atomic membranes, ACS Appl. Mater. Interfaces 12 (2020) 10801–10808.
- [20] M.T. Hwang, M. Heiranian, Y. Kim, S. You, J. Leem, A. Taqieddin, V. Faramarzi, Y. Jing, I. Park, A.M. van der Zande, S. Nam, N.R. Aluru, R. Bashir, Ultrasensitive detection of nucleic acids using deformed graphene channel field effect biosensors, Nat. Commun. 11 (2020) 1543.
- [21] S. Lim, H. Luan, S. Zhao, Y. Lee, Y. Zhang, Y. Huang, J.A. Rogers, J.-H. Ahn, Assembly of foldable 3d microstructures using graphene hinges, Adv. Mater. 32 (28) (2020) 2001303.
- [22] H. Zhao, K. Li, M. Han, F. Zhu, A. Vázquez-Guardado, P. Guo, Z. Xie, Y. Park, L. Chen, X. Wang, H. Luan, Y. Yang, H. Wang, C. Liang, Y. Xue, R.D. Schaller, D. Chanda, Y. Huang, Y. Zhang, J.A. Rogers, Buckling and twisting of advanced materials into morphable 3d mesostructures, Proc. Nat. Acad. Sci. 116 (27) (2019) 13239–13248.
- [23] W. Lee, Y. Liu, Y. Lee, B.K. Sharma, S.M. Shinde, S.D. Kim, K. Nan, Z. Yan, M. Han, Y. Huang, Y. Zhang, J.-H. Ahn, J.A. Rogers, Two-dimensional materials in functional three-dimensional architectures with applications in photodetection and imaging, Nat. Commun. 9 (2018) 1417.
- [24] D. Nandwana, E. Ertekin, Ripples, strain, and misfit dislocations: Structure of graphene-boron nitride superlattice interfaces, Nano Lett. 15 (2015) 1468–1475.
- [25] D. Nandwana, E. Ertekin, Lattice mismatch induced ripples and wrinkles in planar graphene/boron nitride superlattices, J. Appl. Phys. 117 (23) (2015) 234304.
- [26] B.C. McGuigan, P. Pochet, H.T. Johnson, Critical thickness for interface misfit dislocation formation in two-dimensional materials, Phys. Rev. B 93 (2016) 214102
- [27] X. Duan, C. Wang, J.C. Shaw, R. Cheng, Y. Chen, H. Li, X. Wu, Y. Tang, Q. Zhang, A. Pan, J. Jiang, R. Yu, Y. Huang, X. Duan, Lateral epitaxial growth of twodimensional layered semiconductor heterojunctions, Nat. Nanotechnol. 9 (2014) 1024–1030.

- [28] Y. Kobayashi, S. Yoshida, M. Maruyama, K. Murase, Y. Maniwa, O. Takeuchi, S. Okada, H. Shigekawa, Y. Miyata, Growth and characterization of in-plane heterostructures based on two-dimensional materials, in: 2019 Electron Devices Technology and Manufacturing Conference (EDTM), 2019, pp. 270–272.
- [29] J. Berry, S. Ristić, S. Zhou, J. Park, D.J. Srolovitz, The MoSeS dynamic omnigami paradigm for smart shape and composition programmable 2D materials, Nat. Commun. 10 (2019) 5210.
- [30] B. Ni, T. Zhang, J. Li, X. Li, H. Gao, Topological Design of Graphene, ch. 1, pp. 1–44. John Wiley & Sons Ltd, 2019.
- [31] O.V. Yazyev, S.G. Louie, Topological defects in graphene: Dislocations and grain boundaries, Phys. Rev. B 81 (2010) 195420.
- [32] N.D. Mermin, The topological theory of defects in ordered media, Rev. Mod. Phys. 51 (1979) 591–648.
- [33] J.F. Sadoc, R. Mosseri, Geometrical Frustration. Collection Alea-Saclay: Monographs and Texts in Statistical Physics, Cambridge University Press, 2006.
- [34] J.P. Sethna, "Order parameters, broken symmetry, and topology," 1992.
- [35] M. Toulouse, G. Kléman, Principles of a classification of defects in ordered media, J. de Physique Lett. 37 (1976) 149–151.
- [36] V. Volovik, G.E. Mineev, Vortices with free ends in superfluid 3he-a, JETP Lett 23 (1976) 593–595.
- [37] D. Rogula, Trends in application of pure mathematics to mechanics, Pitman, London, 1976.
- [38] N. Blackett, Disclination lines in glasses, Philos. Magaz. A. 40 (1979) 859-868.
- [39] D.R. Nelson, M. Widom, Symmetry, landau theory and polytope models of glass, Nucl. Phys. B 240 (1) (1984) 113–139.
- [40] D. Nelson, Defects and Geometry in Condensed Matter Physics, Cambridge University Press, 2002.
- [41] D.R. Nelson, B.I. Halperin, Dislocation-mediated melting in two dimensions, Phys. Rev. B 19 (1979) 2457–2484.
- [42] H.S. Seung, D.R. Nelson, Defects in flexible membranes with crystalline order, Phys. Rev. A 38 (1988) 1005–1018.
- [43] A. Föppl, Vorlesungen über technische Mechanik, BG Teubner 6 (1910).
- [44] T.V. Kármán, Festigkeitsprobleme im maschinenbau, in: Mechanik, Springer, 1907, pp. 311–385.
- [45] M.K. Blees, A.W. Barnard, P.A. Rose, S.P. Roberts, K.L. McGill, P.Y. Huang, A. R. Ruyack, J.W. Kevek, B. Kobrin, D.A. Muller, P.L. McEuen, Graphene kirigami, Nature 524 (2015) 204–207.
- [46] H.C. Lee, E.Y. Hsieh, K. Yong, S. Nam, Multiaxially-stretchable kirigami-patterned mesh design for graphene sensor devices, Nano Res. (2020) 1–7.
- [47] D. Akinwande, C.J. Brennan, J.S. Bunch, P. Egberts, J.R. Felts, H. Gao, R. Huang, J.-S. Kim, T. Li, Y. Li, K.M. Liechti, N. Lu, H.S. Park, E.J. Reed, P. Wang, B. I. Yakobson, T. Zhang, Y.-W. Zhang, Y. Zhou, Y. Zhu, A review on mechanics and mechanical properties of 2d materials—graphene and beyond, Extreme Mech. Lett. 13 (2017) 42–77.
- [48] W. Cai, W.D. Nix, Imperfections in Crystalline Solids. MRS-Cambridge Materials Fundamentals, Cambridge University Press, 2016.
- [49] T. Zhang, X. Li, H. Gao, Defects controlled wrinkling and topological design in graphene, J. Mech. Phys. Solids 67 (2014) 2–13.
- [50] K. Kim, Z. Lee, W. Regan, C. Kisielowski, M.F. Crommie, A. Zettl, Grain boundary mapping in polycrystalline graphene, ACS Nano 5 (2011) 2142–2146.
- [51] W. Zhou, X. Zou, S. Najmaei, Z. Liu, Y. Shi, J. Kong, J. Lou, P.M. Ajayan, B. I. Yakobson, J.-C. Idrobo, Intrinsic structural defects in monolayer molybdenum disulfide, Nano Lett. 13 (2013) 2615–2622.
- [52] P.Y. Huang, S. Kurasch, A. Srivastava, V. Skakalova, J. Kotakoski, A. V. Krasheninnikov, R. Hovden, Q. Mao, J.C. Meyer, J. Smet, D.A. Muller, U. Kaiser, Direct imaging of a two-dimensional silica glass on graphene, Nano Lett. 12 (2012) 1081–1086.
- [53] S. Chen, D.C. Chrzan, Continuum theory of dislocations and buckling in graphene, Phys. Rev. B 84 (2011) 214103.
- [54] H. Emmerich, H. Löwen, R. Wittkowski, T. Gruhn, G.I. Tóth, G. Tegze, L. Gránásy, Phase-field-crystal models for condensed matter dynamics on atomic length and diffusive time scales: an overview, Adv. Phys. 61 (6) (2012) 665–743.
- [55] K.R. Elder, M. Katakowski, M. Haataja, M. Grant, Modeling elasticity in crystal growth, Phys. Rev. Lett. 88 (2002) 245701.
- [56] Z.-J. Wang, J. Dong, L. Li, G. Dong, Y. Cui, Y. Yang, W. Wei, R. Blume, Q. Li, L. Wang, X. Xu, K. Liu, C. Barroo, J.W.M. Frenken, Q. Fu, X. Bao, R. Schlögl, F. Ding, M.-G. Willinger, The coalescence behavior of two-dimensional materials revealed by multiscale in situ imaging during chemical vapor deposition growth, ACS Nano 14 (2020) 1902–1918.
- [57] J.C. Meyer, C. Kisielowski, R. Erni, M.D. Rossell, M.F. Crommie, A. Zettl, Direct imaging of lattice atoms and topological defects in graphene membranes, Nano Lett. 8 (2008) 3582–3586.
- [58] Y. Cui, H. Zhang, W. Chen, Z. Yang, Q. Cai, Structural evolution of flower defects and effects on the electronic structures of epitaxial graphene, J. Phys. Chem. C 121 (2017) 15282–15287.
- [59] B.I. Yakobson, F. Ding, Observational geology of graphene, at the nanoscale, ACS Nano 5 (2011) 1569–1574.
- [60] C. Ophus, A. Shekhawat, H. Rasool, A. Zettl, Large-scale experimental and theoretical study of graphene grain boundary structures, Phys. Rev. B 92 (2015) 205402.
- [61] A. Shekhawat, C. Ophus, R.O. Ritchie, A generalized read–shockley model and large scale simulations for the energy and structure of graphene grain boundaries, RSC Adv. 6 (2016) 44489–44497.
- [62] P. Merino, M. Švec, A.L. Pinardi, G. Otero, J.A. Martín-Gago, Strain-driven moiré superstructures of epitaxial graphene on transition metal surfaces, ACS Nano 5 (2011) 5627–5634.

- [63] S. Zhu, P. Pochet, H.T. Johnson, Controlling rotation of two-dimensional material flakes, ACS Nano 13 (2019) 6925–6931.
- [64] A.V. Tyurnina, H. Okuno, P. Pochet, J. Dijon, Cvd graphene recrystallization as a new route to tune graphene structure and properties, Carbon 102 (2016) 400, 505
- [65] P.Y. Huang, C.S. Ruiz-Vargas, A.M. van der Zande, W.S. Whitney, M.P. Levendorf, J.W. Kevek, S. Garg, J.S. Alden, C.J. Hustedt, Y. Zhu, J. Park, P.L. McEuen, D. A. Muller, Grains and grain boundaries in single-layer graphene atomic patchwork quilts, Nature 469 (Jan 2011) 389–392.
- [66] E. Cockayne, G.M. Rutter, N.P. Guisinger, J.N. Crain, P.N. First, J.A. Stroscio, Grain boundary loops in graphene, Phys. Rev. B 83 (2011) 195425.
- [67] A. Cresti, J. Carrete, H. Okuno, T. Wang, G.K. Madsen, N. Mingo, P. Pochet, Growth, charge and thermal transport of flowered graphene, Carbon 161 (2020) 259–268.
- [68] K. Hayashi, S. Sato, N. Yokoyama, Anisotropic graphene growth accompanied by step bunching on a dynamic copper surface, Nanotechnology 24 (2012) 025603.
- [69] A. Celis, M.N. Nair, M. Sicot, F. Nicolas, S. Kubsky, A. Taleb-Ibrahimi, D. Malterre, A. Tejeda, Growth, morphology and electronic properties of epitaxial graphene on vicinal ir(332) surface, Nanotechnology 31 (2020) 285601.
- [70] A. Stone, D. Wales, Theoretical studies of icosahedral c60 and some related species, Chem. Phys. Lett. 128 (5) (1986) 501–503.
- [71] J. Ma, D. Alfe, A. Michaelides, E. Wang, Stone-wales defects in graphene and other planar sp²-bonded materials, Phys. Rev. B 80 (2009) 033407.
- [72] E. Ertekin, D.C. Chrzan, M.S. Daw, Topological description of the stone-wales defect formation energy in carbon nanotubes and graphene, Phys. Rev. B 79 (2009) 155421.
- [73] A.W. Robertson, C.S. Allen, Y.A. Wu, K. He, J. Olivier, J. Neethling, A.I. Kirkland, J.H. Warner, Spatial control of defect creation in graphene at the nanoscale, Nat. Commun. 3 (2012) 1144.
- [74] P. Ahlberg, F.O.L. Johansson, Z.-B. Zhang, U. Jansson, S.-L. Zhang, A. Lindblad, T. Nyberg, Defect formation in graphene during low-energy ion bombardment, APL Mater. 4 (4) (2016) 046104.
- [75] J. Zhuang, R. Zhao, J. Dong, T. Yan, F. Ding, Evolution of domains and grain boundaries in graphene: a kinetic monte carlo simulation, Phys. Chem. Chem. Phys. 18 (2016) 2932–2939.
- [76] S. Kurasch, J. Kotakoski, O. Lehtinen, V. Skákalová, J. Smet, C.E. Krill, A. V. Krasheninnikov, U. Kaiser, Atom-by-atom observation of grain boundary migration in graphene, Nano Lett. 12 (2012) 3168–3173.
- [77] B.C. McGuigan, H.T. Johnson, P. Pochet, Coupling point defects and potential energy surface exploration, Comput. Mater. Sci. 166 (2019) 1–8.
- [78] S. Chen, E. Ertekin, D.C. Chrzan, Plasticity in carbon nanotubes: Cooperative conservative dislocation motion, Phys. Rev. B 81 (2010) 155417.
- [79] S. Lee, G.S. Hwang, Valence force field-based monte carlo bond-rotation method for the determination of sp2-bonded carbon structures, J. Appl. Phys. 110 (9) (2011) 093524.
- [80] A.W. Robertson, G.-D. Lee, K. He, Y. Fan, C.S. Allen, S. Lee, H. Kim, E. Yoon, H. Zheng, A.I. Kirkland, J.H. Warner, Partial dislocations in graphene and their atomic level migration dynamics, Nano Lett. 15 (2015) 5950–5955.
- [81] D.G. Kvashnin, P.B. Sorokin, D. Shtansky, D. Golberg, A.V. Krasheninnikov, Line and rotational defects in boron-nitrene: Structure, energetics, and dependence on mechanical strain from first-principles calculations, Phys. Status Solidi (b) 252 (8) (2015) 1725–1730.
- [82] O. Lehtinen, H.-P. Komsa, A. Pulkin, M.B. Whitwick, M.-W. Chen, T. Lehnert, M. J. Mohn, O.V. Yazyev, A. Kis, U. Kaiser, A.V. Krasheninnikov, Atomic scale microstructure and properties of se-deficient two-dimensional mose2, ACS Nano 9 (2015) 3274–3283.
- [83] V.A. Lubarda, Dislocation burgers vector and the peach-koehler force: a review, J. Mater. Res. Technol. 8 (1) (2019) 1550–1565.
- [84] J.P. Hirth, G. Hirth, J. Wang, Disclinations and disconnections in minerals and metals, Proc. Nat. Acad. Sci. 117 (1) (2020) 196–204.
- [85] S. Plimpton, Fast parallel algorithms for short-range molecular dynamics, J. Comput. Phys. 117 (1) (1995) 1–19.
- [86] T.C. O'Connor, J. Andzelm, M.O. Robbins, Airebo-m: A reactive model for hydrocarbons at extreme pressures, J. Chem. Phys. 142 (2) (2015) 024903.
- [87] E. Annevelink, E. Ertekin, H.T. Johnson, Grain boundary structure and migration in graphene via the displacement shift complete lattice, Acta Mater. 166 (2019) 67–74.
- [88] A. Rajabzadeh, F. Mompiou, M. Legros, N. Combe, Elementary mechanisms of shear-coupled grain boundary migration, Phys. Rev. Lett. 110 (2013) 265507.
- [89] S.L. Thomas, K. Chen, J. Han, P.K. Purohit, D.J. Srolovitz, Reconciling grain growth and shear-coupled grain boundary migration, Nat. Commun. 8 (2017) 1764
- [90] S. Maeda, K. Ohno, Global mapping of equilibrium and transition structures on potential energy surfaces by the scaled hypersphere search method: applications to ab initio surfaces of formaldehyde and propyne molecules, J. Phys. Chem. A 109 (2005) 5742–5753.
- [91] C.E. Rasmussen, Gaussian processes in machine learning, in: Summer School on Machine Learning, Springer, 2003, pp. 63–71.
- [92] M.L. Stein, Interpolation of spatial data: some theory for kriging, Springer Science & Business Media, 2012.
- [93] G.H. Teichert, K. Garikipati, Machine learning materials physics: Surrogate optimization and multi-fidelity algorithms predict precipitate morphology in an alternative to phase field dynamics, Comput. Methods Appl. Mech. Eng. 344 (2019) 666–693.

- [94] S. Goedecker, Minima hopping: An efficient search method for the global minimum of the potential energy surface of complex molecular systems, J. Chem. Phys. 120 (21) (2004) 9911–9917.
- [95] G. Henkelman, H. Jónsson, Improved tangent estimate in the nudged elastic band method for finding minimum energy paths and saddle points, J. Chem. Phys. 113 (22) (2000) 9978–9985.
- [96] G. Henkelman, B.P. Uberuaga, H. Jónsson, A climbing image nudged elastic band method for finding saddle points and minimum energy paths, J. Chem. Phys. 113 (22) (2000) 9901–9904.
- [97] K. Kanamori, K. Toyoura, J. Honda, K. Hattori, A. Seko, M. Karasuyama, K. Shitara, M. Shiga, A. Kuwabara, I. Takeuchi, Exploring a potential energy surface by machine learning for characterizing atomic transport, Phys. Rev. B 97 (2018) 125124.
- [98] V. Kaibel, M.A. Peinhardy, "On the bottleneck shortest path problem," Konrad-Zuse-Zentrum f
 ür Informationstechnik, 2006.
- [99] G. Chaslot, S. Bakkes, I. Szita, P. Spronck, Monte-carlo tree search: A new framework for game ai, AIIDE (2008).
- [100] C.B. Browne, E. Powley, D. Whitehouse, S.M. Lucas, P.I. Cowling, P. Rohlfshagen, S. Tavener, D. Perez, S. Samothrakis, S. Colton, A survey of monte carlo tree search methods, IEEE Trans. Comput. Intell. AI in Games 4 (1) (2012) 1–43.
- [101] S. Gelly, L. Kocsis, M. Schoenauer, M. Sebag, D. Silver, C. Szepesvári, O. Teytaud, The grand challenge of computer go: Monte carlo tree search and extensions, Commun. ACM 55 (2012) 106–113.
- [102] X. Yang, J. Zhang, K. Yoshizoe, K. Terayama, K. Tsuda, Chemts: an efficient python library for de novo molecular generation, Sci. Technol. Adv. Mater. 18 (1) (2017) 972–976. PMID: 29435094.
- [103] M.H.S. Segler, M. Preuss, M.P. Waller, Planning chemical syntheses with deep neural networks and symbolic ai, Nature 555 (2018) 604–610.
- [104] S. Kajita, T. Kinjo, T. Nishi, Autonomous molecular design by monte-carlo tree search and rapid evaluations using molecular dynamics simulations, Commun. Phys. 3 (2020) 77.
- [105] D. Silver, T. Hubert, J. Schrittwieser, I. Antonoglou, M. Lai, A. Guez, M. Lanctot, L. Sifre, D. Kumaran, T. Graepel, T. Lillicrap, K. Simonyan, D. Hassabis, A general reinforcement learning algorithm that masters chess, shogi, and go through selfplay, Science 362 (6419) (2018) 1140–1144.
- [106] Y. Kim, N. Nakata, Geophysical inversion versus machine learning in inverse problems, Lead. Edge 37 (12) (2018) 894–901.
- [107] H. Li, J. Schwab, S. Antholzer, M. Haltmeier, "NETT: solving inverse problems with deep neural networks," jun, Inverse Prob. 36 (2020) 065005.
- [108] D. Whitley, A genetic algorithm tutorial, Stat. Comput. 4 (2) (1994) 65-85.
- [109] F. Scarselli, M. Gori, A.C. Tsoi, M. Hagenbuchner, G. Monfardini, The graph neural network model, IEEE Trans. Neural Networks 20 (1) (2008) 61–80.
- [110] T. Xie, J.C. Grossman, Crystal graph convolutional neural networks for an accurate and interpretable prediction of material properties, Phys. Rev. Lett. 120 (14) (2018) 145301.
- [111] C.W. Park, C. Wolverton, Developing an improved crystal graph convolutional neural network framework for accelerated materials discovery, Phys. Rev. Mater. 4 (6) (2020) 063801.
- [112] O. Ronneberger, P. Fischer, T. Brox, U-net: Convolutional networks for biomedical image segmentation, in: International Conference on Medical image computing and computer-assisted intervention, Springer, 2015, pp. 234–241.
- [113] Ö. Çiçek, A. Abdulkadir, S.S. Lienkamp, T. Brox, O. Ronneberger, 3d u-net: learning dense volumetric segmentation from sparse annotation, in: International conference on medical image computing and computer-assisted intervention, Springer, 2016, pp. 424–432.
- [114] O. Lehtinen, S. Kurasch, A.V. Krasheninnikov, U. Kaiser, Atomic scale study of the life cycle of a dislocation in graphene from birth to annihilation, Nat. Commun. 4 (2013) 2098
- [115] C. Gong, K. He, Q. Chen, A.W. Robertson, J.H. Warner, In situ high temperature atomic level studies of large closed grain boundary loops in graphene, ACS Nano 10 (2016) 9165–9173.
- [116] S. Zhu, Y. Huang, N.N. Klimov, D.B. Newell, N.B. Zhitenev, J.A. Stroscio, S. D. Solares, T. Li, Pseudomagnetic fields in a locally strained graphene drumhead, Phys. Rev. B 90 (2014) 075426.
- [117] G. López-Polín, M. Jaafar, F. Guinea, R. Roldán, C. Gómez-Navarro, J. Gómez-Herrero, The influence of strain on the elastic constants of graphene, Carbon 124 (2017) 42–48.
- [118] S. Kim, E. Annevelink, E. Han, J. Yu, P.Y. Huang, E. Ertekin, A.M. van der Zande, Stochastic stress jumps due to soliton dynamics in two-dimensional van der waals interfaces, Nano Lett. 20 (Feb 2020) 1201–1207.
- [119] C.-W. Kuo, J.-Y. Shiu, P. Chen, G.A. Somorjai, Fabrication of size-tunable largearea periodic silicon nanopillar arrays with sub-10-nm resolution, J. Phys. Chem. B 107 (2003) 9950–9953.
- [120] A. Dong, J. Chen, P.M. Vora, J.M. Kikkawa, C.B. Murray, Binary nanocrystal superlattice membranes self-assembled at the liquid–air interface, Nature 466 (2010) 474–477.
- [121] M.R. Rosenberger, H.-J. Chuang, K.M. McCreary, A.T. Hanbicki, S.V. Sivaram, B. T. Jonker, Nano-"squeegee" for the creation of clean 2d material interfaces, ACS Appl. Mater. Interfaces 10 (2018) 10379–10387.
- [122] P. Schweizer, C. Dolle, E. Spiecker, "In situ manipulation and switching of dislocations in bilayer graphene," Sci. Adv., vol. 4, no. 8, 2018.
- [123] C.-H. Lee, A. Khan, D. Luo, T.P. Santos, C. Shi, B.E. Janicek, S. Kang, W. Zhu, N. A. Sobh, A. Schleife, B.K. Clark, P.Y. Huang, Deep learning enabled strain mapping of single-atom defects in two-dimensional transition metal dichalcogenides with sub-picometer precision, Nano Lett. 20 (2020) 3369–3377.